Thermal Mechanical Assessment of a SiC-SiC-Composite Clad Fuel Pin Concept in a Light Water Reactor Environment*

John Alvis[1,b], Gyanender Singh[a], Kyle Gamble[a], David Kamerman[b], Seokbin Seo[b], and Katheren Nantes[c]

[a]Computational Mechanics and Materials, Idaho National Laboratory, Idaho Falls, ID, USA
[b]Fuel Performance Development and Qualification, Idaho National Laboratory, Idaho Falls, ID, USA
[c]Department of Nuclear Engineering, Pennsylvania State University, University Park, PA, USA

[1] Corresponding author: john.alvis@inl.gov

Thermal Mechanical Assessment of a SiC-SiC-Composite Clad Fuel Pin Concept in a Light Water Reactor Environment*

John Alvis[1,b], Gyanender Singh[a], Kyle Gamble[a], David Kamerman[b], Seokbin Seo[b], and Katheren Nantes[c]

[a]Computational Mechanics and Materials, Idaho National Laboratory, Idaho Falls, ID, USA
[b]Fuel Performance Development and Qualification, Idaho National Laboratory, Idaho Falls, ID, USA
[c]Department of Nuclear Engineering, Pennsylvania State University, University Park, PA, USA

Abstract

Accident-tolerant fuels (ATFs) are designed to increase coping time following an accident scenario while preserving or improving current steady-state reactor operational performance. A potential ATF concept is using silicon carbide (SiC)-SiC-composite claddings. Fuel-performance simulations were conducted on a SiC-SiC-based cladding concept utilizing a multilayered approach for improved performance. This cladding concept is referred to in this paper as "the duplex concept" as it is a duplex structure composed of a monolithic SiC layer placed on the outside of an inner SiC-SiC composite layer. The monolithic SiC layer is used to provide gas tightness to the rod and protect the SiC-SiC-composite layer from exposure to the coolant. A liquid metal is added to the fuel-cladding gap for improved thermal transport between the fuel and the cladding. In this work, the BISON fuel-performance code was used to conduct fuel-performance simulations on the cladding concept. Comparisons are made with a current prototypic fuel-rod design consisting of uranium dioxide (UO_2) fuel enclosed in Zircaloy-4 cladding under four relevant conditions. For condition I (normal operations) two representative steady-state cases were considered, one with a constant rod average heat rate, and one with an initially higher heat rate. For condition II events, a pellet-cladding interaction (PCI) ramp case was simulated to analyze potential anticipated operational occurrences. Condition III/IV transient responses during a loss of coolant accident (LOCA) and a reactivity-initiated accident (RIA) were also simulated. This computational study demonstrated that for normal operating conditions, the SiC concept cladding performed as well as the baseline for the standard-power cases evaluated. The ramping evaluations indicate potential for earlier fracturing of the SiC-SiC composite cladding compared to the Zircaloy-4 cladding due to the temperature gradient and the subsequent differential thermal conductivity degradation and swelling across the composite thickness. In condition III/IV events the SiC-SiC duplex concept remains intact after a 700 J/g RIA similar to Zircaloy-4 fuel systems. Under LOCA conditions, the duplex concept showed significantly improved performance, remaining intact in contrast to Zircaloy-4 which ballons and bursts.

Keywords: silicon carbide (SiC), accident-tolerant fuel (ATF), cladding, light-water reactor (LWR), nuclear, BISON computing code, fuel performance

1 INTRODUCTION AND BACKGROUND

Currently licensed fuel designs in the United States (U.S.) for the light-water reactor (LWR) fleet uses uranium dioxide (UO_2) fuel, enclosed within a zirconium-alloy cladding. Years of research, accompanied by over 60 years of reactor operational experience, have steadily generated technological advancements, as well as an extensive experience base, of both material response and performance in commercial and

[1] Corresponding author: john.alvis@inl.gov

test-reactor data for steady-state and transient conditions. However, the earthquake and subsequent tsunami at the Fukushima Daiichi nuclear power generating station, coupled with recent material advancements, have provided a strong motivation for the industry and regulatory agencies to develop new fuel designs with an emphasis on improving performance, safety, and reliability in both operating and accident scenarios. These new fuel designs are referred to as accident-tolerant fuels (ATFs).

Silicon carbide (SiC) has been investigated for use in both fission and fusion applications and has been considered as a candidate material for ATF cladding in LWRs [1][2]. High-purity, crystalline SiC is a very stable material under neutron irradiation, undergoing only minimal swelling and strength changes to 40 dpa and higher, which represents many times the exposure for fuel life in a typical LWR. In addition, SiC retains its mechanical properties at high temperatures and reacts more slowly with steam than zirconium alloys. However, monolithic SiC alone has low fracture toughness, making it unsuitable for nuclear-cladding applications where fuel containment is essential and a coolable geometry must be maintained, especially under transient or off-normal conditions. The solution is to employ an engineered composite structure to address this brittleness, using strong SiC fibers that reinforce a SiC matrix to form a SiC-SiC composite. Compared to monolithic SiC, these composites offer improved fracture toughness and pseudo-ductility. High-purity, radiation-tolerant SiC composites for nuclear applications are typically fabricated using chemical vapor infiltration (CVI) [3][7].

SiC-based cladding properties are highly dependent on the processing route used, particularly for any fiber-reinforced composite layers. In addition, while SiC-SiC composites undergo pseudo-ductile fracture, rather than brittle failure. During this pseudo-ductile fracture, extensive microcracking occurs, which can lead to a loss of hermeticity. Microcracking can occur at strains less than 1% [4][28], below the level at which zirconium-alloy cladding would exhibit any plastic deformation. Accordingly, careful development of SiC-based cladding designs is needed to mitigate microcracking and ensure hermeticity.

As a step to expedite the licensing process required before any ATF concept can be deployed, the thermal-mechanical fuel performance of advanced SiC-SiC cladding concepts in condition I (normal operations), condition II (anticipated operational occurrences (AOOs)) and condition III/IV (design basis accidents/transients (e.g., LOCA, RIA)) will have to be assessed. This paper evaluates the performance of a full-length fuel-pin design with SiC-SiC cladding incorporating different features meant to mitigate the potential for a loss of hermeticity due to microcracking using the BISON fuel-performance code [5]. The SiC-SiC clad fuel-pin design uses a monolithic outer layer of SiC, and a low melting point liquid-metal bond between the fuel and the cladding. This architecture can be seen in Figure 1 and can be characterized as a duplex architecture. The impact of this architecture on the fuel temperature, plenum pressure, SiC-SiC cladding stress, and SiC-SiC cladding strain will be assessed using the BISON simulations and compared to those of a standard zirconium-alloy cladding.

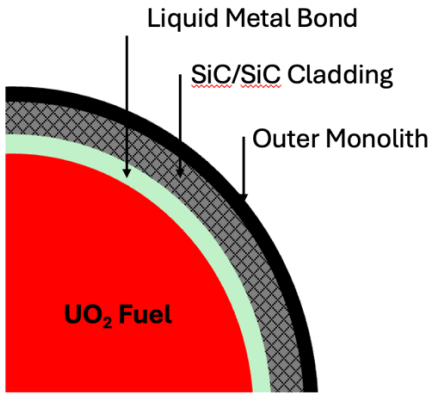

Figure 1. Fuel-pin design with duplex architecture.

2 Model Description

2.1 Geometry

The simulations will model a SiC-SiC clad fuel pin with a 9.5 mm outer diameter and a 365.76-cm-high fuel column with a 25.4 cm plenum dimensions consistent with a standard 17x17 PWR assembly [6]. For the duplex cladding architecture, radial dimensions used in the simulation are shown in Table 1 and compared with the standard Zircaloy-4 (Zr-4) pin.

Table 1. Radial dimensions and Internal Pressure of the fuel pins (units: mm).

	SiC-SiC Duplex Pin	Standard 17x17 Zr-4 Pin
Fuel pellet outer radius (mm)	3.95	4.095
Cladding inner radius (mm)	4.05	4.184
SiC-SiC-composite outer radius (mm)	4.65	Not applicable
Cladding outer radius (mm)	4.75	4.75 (outer radius)
Plenum Pressure (MPa)	0.1 MPa	2.0 MPa

For ceramic composite materials like SiC-SiC tubing, thicker materials will be more challenged from thermal- and irradiation-swelling loads, while thinner materials will be more challenged from mechanical loads. No attempts are made as a part of this initial study to optimize the geometry of the duplex architecture to maximize its performance. It is acknowledged that more optimized geometries could have an impact on the results. It is also possible that the ability to fabricate a composite architecture within a given dimensional tolerance with reliable material properties may limit the fuel-rod design such that the dimensions used in this study are unrealistic. However, it is the purpose of this study to illustrate the strengths and weaknesses of the duplex architecture in different operating conditions relative to a standard Zr-4 pin such that later design efforts can optimize the geometry around fabrication limitations and necessary performance in operating conditions.

The BISON fuel-performance code represents these geometries using an axisymmetric (2D-RZ) finite element mesh of the fuel rods. In this representation, a mesh of one-half of the fuel rod is modeled with azimuthal symmetry being assumed about the cylindrical centerline of the rod. The mesh of the duplex SiC-SiC composite cladding and baseline Zr-4 cladding with the fuel are shown in Figure 2. The duplex cladding mesh had 1000 elements in the axial direction; radially, the CVD SiC and composite SiC layers had two and four elements, respectively. The baseline Zr-4 cladding had 1000 and four elements in the axial and radial directions, respectively. The liquid tin bond reduces the available plenum and this decrease in the plenum has been accounted for in the simulation for calculation of plenum volume and plenum pressure.

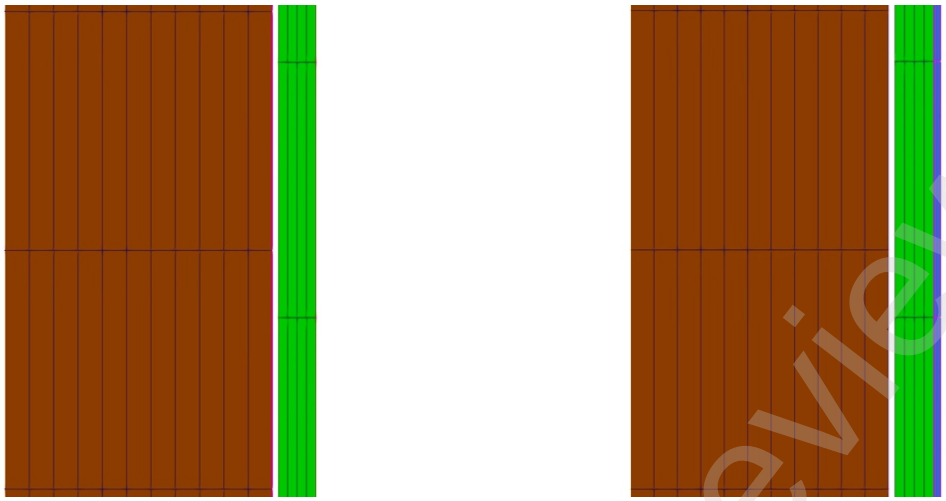

(a) (b)

Figure 2. Meshes of (a) Zr-4 and (b) duplex SiC cladding models.

2.2 Constitutive Models

Cladding material undergoes deformation in several different ways in a reactor environment. Under the effect of irradiation, the material may swell (increasing volume), grow (with conserved volume), or experience enhanced creep due to applied loads over long times. Simultaneously it may undergo regular thermal expansion as well as elastic and plastic deformation in response to applied loadings. The total strain (e) can be expressed as the sum of swelling/irradiation growth ($\boldsymbol{e}_s$), creep strain ($\boldsymbol{e}_c$), thermal expansion strain ($\boldsymbol{e}_t$), elastic strain ($\boldsymbol{e}_e$), and plastic strain ($\boldsymbol{e}_p$), as indicated in Equation (1):

$$\boldsymbol{e} = \boldsymbol{e}_s + \boldsymbol{e}_c + \boldsymbol{e}_t + \boldsymbol{e}_e + \boldsymbol{e}_p \tag{1}$$

Using Hooke's law, as shown in Equation (2), the stress in the cladding is calculated where $\boldsymbol{s}$ is the stress and $\boldsymbol{D}$ is the elastic stiffness of the material:

$$\boldsymbol{s} = \boldsymbol{D}\boldsymbol{e}_e \tag{2}$$

The SiC-SiC-composite is elastically orthotropic, and the constitutive equation (2) can be expressed in component form as Equations (3), (4), and (5) where r, y, and θ are subscripted:

$$\begin{bmatrix}\sigma_{rr}\\ \sigma_{\theta\theta}\\ \sigma_{yy}\\ \sigma_{\theta y}\\ \sigma_{yr}\\ \sigma_{r\theta}\end{bmatrix} = \begin{bmatrix} \frac{1-\nu_{\theta y}\nu_{y\theta}}{E_\theta E_y \eta} & \frac{\nu_{\theta r}+\nu_{yr}\nu_{\theta y}}{E_\theta E_y \eta} & \frac{\nu_{yr}+\nu_{\theta r}\nu_{y\theta}}{E_\theta E_y \eta} & 0 & 0 & 0 \\ \frac{\nu_{r\theta}+\nu_{ry}\nu_{y\theta}}{E_y E_r \eta} & \frac{1-\nu_{yr}\nu_{ry}}{E_y E_r \eta} & \frac{\nu_{y\theta}+\nu_{yr}\nu_{r\theta}}{E_y E_r \eta} & 0 & 0 & 0 \\ \frac{\nu_{ry}+\nu_{r\theta}\nu_{\theta y}}{E_r E_\theta \eta} & \frac{\nu_{\theta y}+\nu_{ry}\nu_{\theta r}}{E_r E_\theta \eta} & \frac{1-\nu_{r\theta}\nu_{\theta r}}{E_r E_\theta \eta} & 0 & 0 & 0 \\ 0 & 0 & 0 & 2G_{\theta y} & 0 & 0 \\ 0 & 0 & 0 & 0 & 2G_{yr} & 0 \\ 0 & 0 & 0 & 0 & 0 & 2G_{r\theta} \end{bmatrix} \begin{bmatrix}\varepsilon_{rr}\\ \varepsilon_{\theta\theta}\\ \varepsilon_{yy}\\ \varepsilon_{\theta y}\\ \varepsilon_{yr}\\ \varepsilon_{r\theta}\end{bmatrix} \tag{3}$$

where η is:

$$\eta = \frac{1 - \nu_{r\theta}\nu_{\theta r} - \nu_{\theta y}\nu_{y\theta} - \nu_{yr}\nu_{ry} - 2\nu_{r\theta}\nu_{\theta y}\nu_{yr}}{E_r E_\theta E_y} \tag{4}$$

and

$$\frac{\nu_{r\theta}}{E_r} = \frac{\nu_{\theta r}}{E_\theta} \qquad \frac{\nu_{ry}}{E_r} = \frac{\nu_{yr}}{E_y} \qquad \frac{\nu_{y\theta}}{E_y} = \frac{\nu_{\theta y}}{E_\theta} \tag{5}$$

Heat flow through and out of the cladding are computed using the standard Fourier's law, as given in Equation (6), and the convective boundary condition at the surface, as shown in Equation (7), respectively, where $\boldsymbol{q}$ is the heat flux vector, $\boldsymbol{k}$ is the thermal conductivity tensor, $\tilde{\nabla}T$ is the gradient of the temperature, q is the heat flux perpendicular from the surface, T_s is the surface temperature, and T_a is the ambient temperature.

$$\boldsymbol{q} = -\boldsymbol{k}\tilde{\nabla}T \tag{6}$$

$$\dot{q} = h(T_s - T_a) \tag{7}$$

2.3 Material Properties

Conducting accurate thermal mechanical simulations requires the use of accurate material models. For the simulations with the standard Zr-4 clad fuel pin standard material properties from the BISON theory manual are used [18]. For the duplex SiC-SiC clad pin a description of the material models used is described in the following sections. Table 2 summarizes the dependence of SiC-SiC properties on the temperature and irradiation.

Table 2. Dependence of SiC-SiC properties on the temperature and irradiation.

Material Property	**Temperature Dependence**	**Effect of Irradiation**
Specific heat capacity	Dependent [8]	Negligible [8]
Thermal conductivity	Dependent [10],[20]	Strong effect [8],[7]
Coefficient of thermal expansion	Dependent [7]	Negligible.
Young's moduli	Dependent [10],[9]	Dependent [10],[9]
Proportional Stress Limit	Not dependent	Not dependent
Irradiation swelling	Dependent [7]	Dependent [7]
Oxidation	Dependent [10]	Not considered.

2.3.1 Specific Heat Capacity

The specific heat of the SiC-SiC-composite is deemed to be identical to that of monolithic SiC because the effect of a carbon interphase can be neglected [7]. The specific heat varies significantly with the temperature while its dependence on the irradiation dose is negligible. The temperature-dependent specific heat of the SiC-SiC-composite is expressed in Equation (8), as proposed by Snead et al. [8].

$$C_p = 925.65 + 0.3772T - 7.9259 \times 10^{-5}T^2 - \frac{3.1946 \times 10^7}{T^2} \tag{8}$$

where C_p is the specific heat (J/kg-K) and T is the temperature (K).

2.3.2 Thermal Conductivity

Thermal conductivity of SiC-SiC composites is strongly dependent on the nature of the material (impurities, grain size, etc.), the temperature, and the irradiation dose. Thermal diffusivity for a non-irradiated SiC composite is based on the summarized data presented in Koyanagi et al. [10]. A linear interpolation for the thermal diffusivity values (e.g., 4.5×10^{-6} m^2s^{-1} at 25°C, 2.875×10^{-6} m^2s^{-1} at 300°C, 2.125×10^{-6} m^2s^{-1} at 800°C) is performed to obtain the thermal diffusivity values at any temperature. For temperatures outside the range of 25–800°C, the diffusivity value of the range limit is used. The degradation of thermal conductivity due to irradiation is accounted for and is based on the model presented in Snead et al. (2007) [8]. The major equations of this model are presented below. Further details of this model can be found in Snead et al. [11].

$$\frac{1}{k_{irradiated}} = \frac{1}{k_{unirradiated}} + R_{irradiation} \tag{9}$$

$$R_{irradiation} = 15.11\ \mathrm{e}_{swelling}^{vol} \tag{10}$$

where $R_{irradiation}$ is the thermal resistance due to irradiation-induced changes in the material and $\mathrm{e}_{swelling}^{vol}$ is the irradiation-induced volumetric swelling. Equation (10) is based on Stone et al. [12]. The density of the SiC-SiC composite was assumed to be 2800 kg/m^3.

Thermal conductivity of chemical vapor deposited (CVD) SiC is modeled using the same model as the one used for the SiC-SiC composite [11]; however, the values for $k_{unirradiated}$ and $R_{irradiation}$ are different, as shown in Equations (11) and (12).

$$k_{unirradiated} = \frac{1}{-0.0003 + 1.05'10^{-5}T} \tag{11}$$

$$R_{irradiation} = 0.00135 + 6.13\mathrm{e}_{swelling}^{vol} \tag{12}$$

$$\mathrm{k} = 7.511 + 2.088'10^{-2}\mathrm{T} - 1.450'10^{-5}T^2 + 7.668'10^{-9}T^3(3b) \tag{13}$$

2.3.3 Coefficient of Thermal Expansion

The coefficient of thermal expansion for the SiC-SiC composite has a strong dependence on temperature but is negligibly affected by irradiation. In this analysis, the dependence of the coefficient of thermal expansion on the temperature modeled using Equation (14) is:

$$\alpha = 3.8289 \times 10^{-9}T^3 - 1.2209 \times 10^{-5}T^2 + 1.4350 \times 10^{-2}T - 0.7765\ (293\ K < T < 1273\ K) \tag{14}$$

where α is the thermal expansion coefficient ($10^{-6}/K$).

The coefficient of thermal expansion for the monolithic SiC is also significantly dependent on temperature and is provided in Equation (?):

$$\alpha = \begin{Bmatrix} 3.8289 \times 10^{-9}T^3 - 1.2209 \times 10^{-5}T^2 + 1.4350 \times 10^{-2}T - 0.7765\ (298\ K < T < 1273\ K) \\ 5 \times 10^{-6} \qquad\qquad (1273\ K < T) \end{Bmatrix} \tag{?}$$

2.3.4 Young's Moduli and Stress Limits

SiC-SiC-composite elasticity has directional dependence due to the orientation of fiber tows and specific architecture. For this analysis, the composite layer is considered to have orthotropic elasticity with the elastic constants listed in Table 3.

Table 3. Elasticity constants for the composite SiC layer.

Elastic Constants	Value	Reference
E_r (GPa)	100	Assumed.
E_y (GPa)	302.24-1.9148b (b = 45°)	[10]
$E_{\mathbf{q}}$ (GPa)	160	[10]
$\mathbf{n}_{y\mathbf{q}}$	0.25	Assumed based on [9]
$\mathbf{n}_{\mathbf{q}r}$	0.13	Assumed based on [9]
$\mathbf{n}_{ry}$	0.13	Assumed based on [9]
$G_{y\mathbf{q}}$ (GPa)	110	Assumed.
$G_{\mathbf{q}r}$ (GPa)	90	Assumed.
G_{ry} (GPa)	90	Assumed.

The effect of irradiation on the elasticity is accounted for using the Equation (15) where D is the elastic stiffness of the irradiated material and D_o is the elastic stiffness of unirradiated material.

$$D = D_o\left(1 - 6\mathrm{e}^{vol}_{swelling}\right) \tag{15}$$

SiC composite undergoes microcracking slightly before the stress nears its proportional limit stress. The microcracking of SiC composite is exhibited as a pseudo ductile behavior in the stress strain response of the material. The pseudo ductile behavior of composite SiC was modeled using the Hill plasticity model available in the MOOSE framework [18]]. The values of the parameters used in the model [26, 27] are listed in Table 4.

Table 4: Parameters used for the pseudo ductility model based on Hill's yield criterion [26, 27].

Parameter	Value
F, H	0.5
G	0.25
L, M, N	1.5
Yield stress	70 MPa
Hardening constant	1.5×10^{10}
Hardening exponent	1.0

2.3.5 Irradiation-Induced Swelling

The SiC-SiC composite undergoes swelling when subjected to irradiation. This swelling saturates around 1–2 dpa depending on irradiation temperature and is inversely correlated with the temperature.

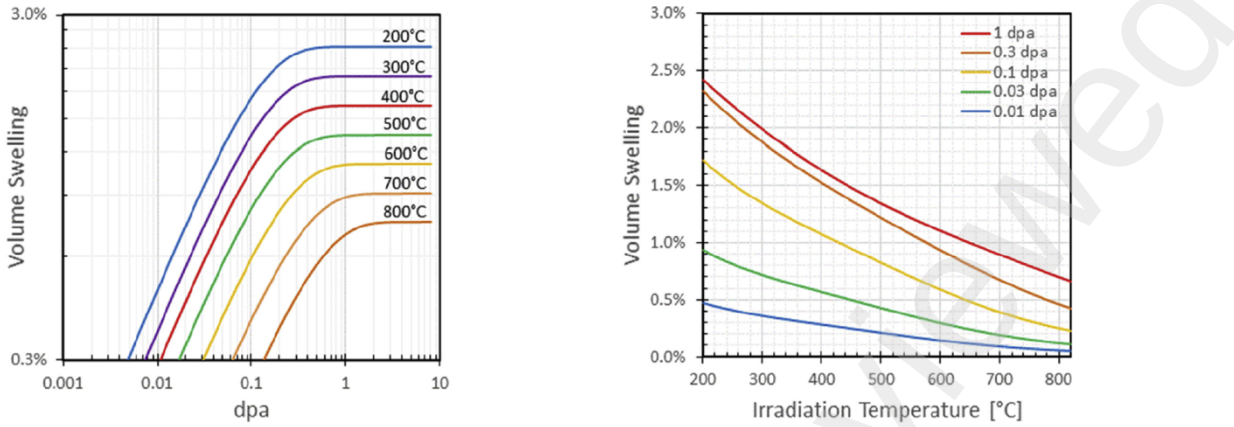

(a) (b)

Figure 3. Volumetric swelling of irradiated CVD SiC and CVI SiC-SiC specimens as a function of (a) dose and (b) temperature [15].

Katoh et al. [7]describes the transient swelling rate of the SiC composite in Equation (16), assuming isothermal irradiation.

$$\dot{S} = k_s \gamma^{-1/3} exp\left(-\frac{\gamma}{\gamma_{sc}}\right) \tag{16}$$

where S is transient swelling rate (%/s), k_s is a rate constant, γ is the neutron fluence dose (dpa), and γ_{sc} is a characteristic saturation dose defined as Equation (17),

$$\gamma_{sc} = 6.7221 \times 10^{-12} T^4 - 1.3095 \times 10^{-8} T^3 + 9.4807 \times 10^{-6} T^2 - 2.7651 \times 10^{-3} T + 0.51801 \tag{17}$$

Later, the original expression was modified to account for three dimensional changes, as indicated in Equations (18), (19), and (20).

$$S = S_s\left[1 - exp\left(1 - \frac{\gamma}{\gamma_c}\right)\right]^{2/3} \tag{18}$$

where S is the volumetric swelling (%), γ_c is characteristic saturation dose (dpa), and S_s is the saturation swelling (%).

$$\gamma_c = 2.9754 \times 10^{-9} T^3 - 5.3970 \times 10^{-6} T^2 + 3.3342 \times 10^{-3} T - 0.57533 \tag{19}$$

$$S_s = -1.8152 \times 10^{-11} T^3 + 6.9368 \times 10^{-8} T^2 - 1.0089 \times 10^{-4} T + 5.8366 \times 10^{-2} \tag{20}$$

3 Light Water Reactor Simulation Conditions

Fuel-performance simulations were performed for the duplex SiC-SiC clad concept and a baseline Zr-4 cladding. Two different normal operating conditions were considered: (1) steady-state operation with a constant rod average linear heat rate of 22 kW/m out to 62 GWd/MTU rod average burnup and, (2) steady-state operation with a rod average linear heat rate of 35 kW/m for up to 20 GWd/MTU rod average burnup followed by operation at a rod average linear heat rate of 22 kW/m to 62 GWd/MTU rod average burnup. A condition II (anticipated operational occurrence) power ramp was simulated following steady-state operation with a rod average linear heat rate of 22 kW/m for up to 20 GWd/MTU rod average burnup. After reaching 20 GWD/MTU the fuel rod experiences a power ramp to rod average heat rate of

45 kW/m in 1 hour and then the power held constant at 45 kW/m for the next 12 hours. These power histories are shown below in Figure 4. The difference between the duplex and baseline irradiation times to get to the same equivalent burnup is due to the difference in the fuel pellet dimensions.

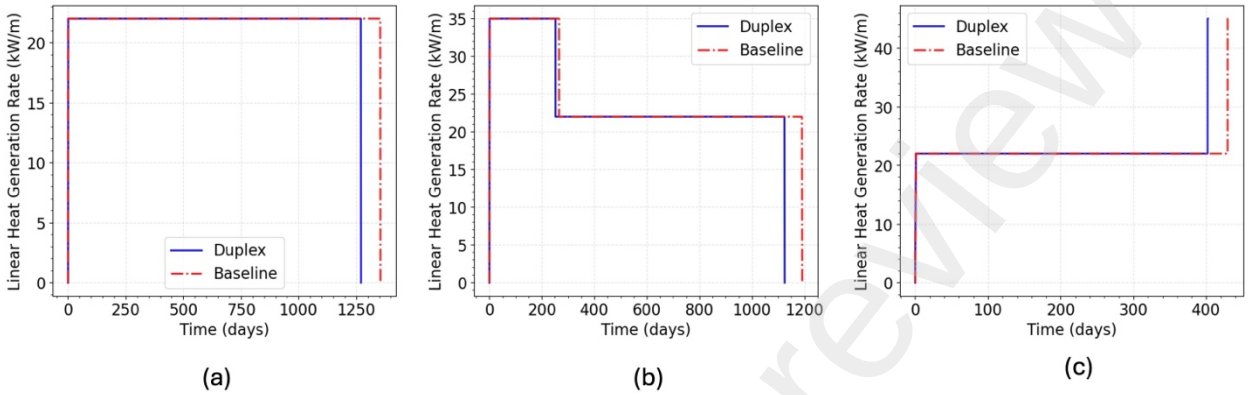

Figure 4. The linear heat generation rate assumed for the three analyses.

The first design-basis accident (DBA) considered in this work is an evaluation of an RIA with energy deposition of 700 J/g. It was performed with a power profile that is Gaussian in shape, with a full-width half-max of 40 ms. The simulation is performed with beginning-of-life (BOL) RIA on fresh fuel at hot zero power conditions. The second DBA considered evaluation of LOCAs at the BOL and EOL.

Power profile: The constant power profile assumed for the fuel rod is shown in Figure 5. This power profile is a representative power profile in the fuel rod with lower power at the ends and higher power towards the center.

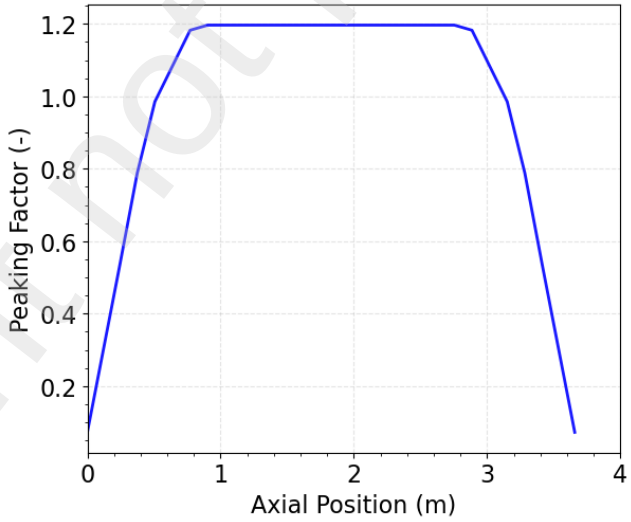

Figure 5. The linear power peaking factor of the fuel rod assumed for all cases.

The outer surface of the cladding temperature was prescribed using the temperature boundary condition obtained from a thermal-hydraulics analysis in both steady state and LOCA conditions. For the RIA case, the cladding temperature was prescribed the same values as for the steady state simulations. The thermal-hydraulic responses of fuel system was evaluated using the Reactor Excursion and Leak Analysis Program (RELAP5-3D) system-level code developed at Idaho National Laboratory (INL) [21].

RELAP5-3D employs a partially implicit numerical scheme to solve partial differential equations for mass, momentum, and energy for a two-phase system based on a nonhomogeneous and nonequilibrium model. In this study, a typical 4-loop Westinghouse PWR was simulated in RELAP5-3D consisting of reactor core and primary coolant loops, including coolant pumps, steam generators, a pressurizer, and the emergency core cooling system. The steady-state conditions were set to generic PWR coolant conditions with a rated power of 3626 MW, as listed in Table 5.

Table 5. Typical reactor conditions.

	PWR
Coolant Mass Flux	2.55 × 106 lb/ft^2-hr (3466 kg/m^2-s)
Water Condition	Liquid water from 550°F (288°C) to 610°F (321°C) at 2250 psi (15.5 MPa)
Rated power	3626 MW

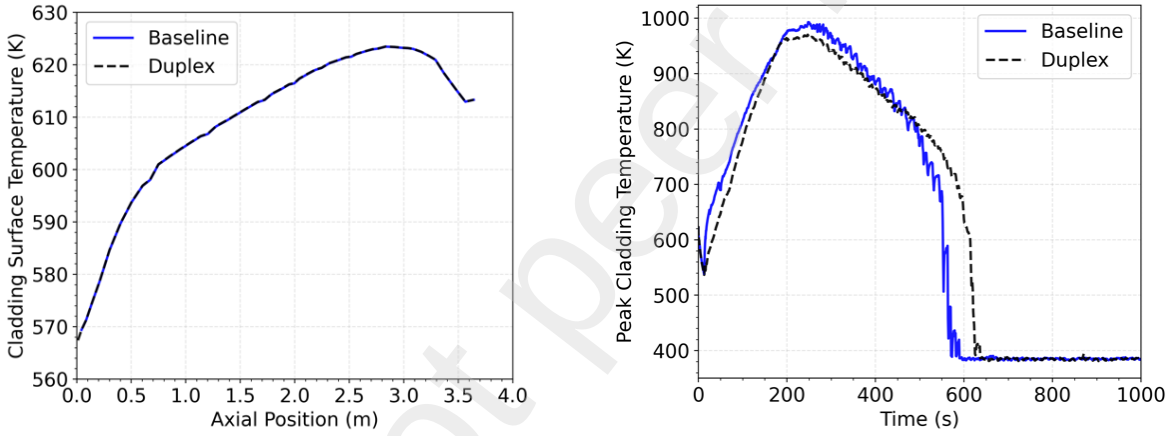

(a) (b)

Figure 6. (a) Axial temperature profile of cladding outer surface at the steady-state condition. (b) Time evolution of the peak cladding temperature during the LOCA.

Figure 6(a) presents the steady-state results of the cladding outer surface temperature along the axial direction during normal operations. The cladding surface temperature that increased along the axial length is due to the heat transfer to the coolant flowing upward. A small decrease in the cladding surface temperature is observed in the plenum region.

Figure 6(b) presents the evolution of the peak cladding temperature as a function of time for the considered LOCA transient. Given the postulated scenario, the cold leg broke at 0.01 s and the scram initiated due to a low-pressure signal at ~ 3.5 s. The power, then, started to decay, which led to the decrease of fuel temperature. Shortly afterward, the stored energy along with the decay energy heated up the fuel to the maximum value during the blowdown phase. Both the fuel and the cladding temperatures inflected once the core was reflooded, and finally got to the rewetting point. Zr-4 and duplex SiC-SiC cladding exhibit a similar history of fuel-centerline temperature. High thermal conductivity of liquid metal gap and high heat capacity of SiC for the duplex concept yielded a slightly lower peak cladding temperature, despite the low thermal conductivity of SiC which impedes the heat transfer from the fuel. This profile is sinusoidal in nature with the ends of the rod set 200°C less than the peak at any given time.

4 RESULTS

The fuel-performance comparisons include the time evolution of fuel-centerline temperature, rod internal pressure, fission gas release (FGR), cladding stresses, and cladding strain. These metrics were selected to highlight the differences in the performance of the duplex SiC and Zr-4 cladding. The analysis results for temperature, plenum pressure, and FGR for the first, constant power, case are provided in Figure 7, and the hoop strains and stress are presented in Figure 8. The analysis results for the second, higher initial power, case are indicated in Figure 9, and Figure 10. The analysis results for anticipated operational occurrence case of an early-life PCI ramp case are reported in Figure 11, and Figure 12.

4.1 Operation with Steady Power

Results for the steady-state case are shown in Figure 7. The power for this case was held constant at 22 kW/m for the duration of the simulation. Overall, results can be explained based on the unique design of the duplex concept which allows for a relatively linear increase in the fuel-centerline temperature due to the presence of the liquid-metal bond between the fuel and cladding. This bond improves the fuel-cladding gap conductance such that the heat transfer is similar to the closed-gap Zr-4 cladding baseline case. The fuel centerline temperature rises constantly till the end of operation due to decreasing thermal conductivity of the fuel with burnup as shown in Figure 7(a). The RIP versus burnup is presented in Figure 7(b). The duplex case has starting lower pressure due to the lower initial fill gas pressure. Since the SiC cladding has liquid metal bonding, the initial plenum volume is also lower than that in the Zr-4 cladding. The expansion of the fuel due to fission product/gaseous swelling presses the liquid metal into the upper plenum decreasing the available plenum volume for released fission gas. The smaller plenum volume for duplex cladding results in the RIP increasing at a faster rate in the duplex cladding compared to the Zr-4 cladding although fissions gas release is lower for the duplex cladding (figure 7c). These results suggest that there could be an increase in internal pressure with burnups greater than 65 GWd/MTU for duplex as compared to the baseline case. It should be noted that for this simulation, the propensity for the liquid metal to penetrate into the open porosity of either the SiC cladding or the fuel was not modeled. The baseline case performance is as expected, with the change in slope of the temperature at approximately 14 GWd/MTU indicative of fuel-to-cladding mechanical contact being established. The outer monolithic SiC layer in duplex is expected not to lose any mass due to exposure to water given the lower coolant temperatures present during normal operation.

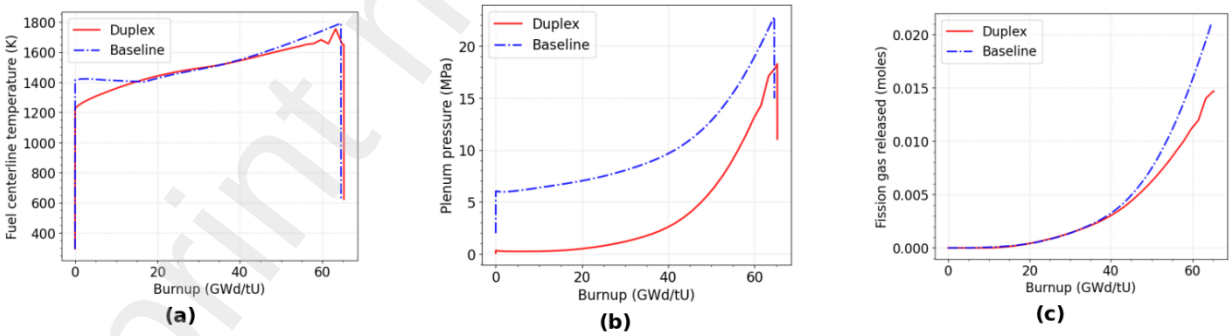

Figure 7. Integral fuel-rod predictions for normal operation: (a) fuel-centerline temperature, (b) rod internal pressure, and (c) fission gas released.

Figure 8(a-b) shows the variation of hoop stresses and strains at the inner and outer surface of the cladding. The hoop strain in the SiC cladding is dominated by the swelling and thermal strains with the swelling strain reaching it saturation value around burnup of 4-6 GWd/MTU. The rapid increase in hoop strain initially is due to irradiation-induced swelling of SiC and thermal expansion. The hoop strain in the

Zr-4 cladding is initially dominated by the creep strain due to Zr-4 cladding "creep down" ultimately making a mechanical contact with the fuel pellet at around 14 GWd/MTU. Once the fuel-cladding gap is closed, cladding deformation is entirely driven by the fuel swelling. This fuel expansion results in increasing hoop strain in the cladding. For the duplex concept, contact between the fuel and cladding occurs much later around 58 GWd/MTU.

Figures 8(c-d) shows the hoop stress versus burnup evolution for the two fuel systems. The baseline case operates under compression due to the coolant pressure acting on the cladding outer surface. The stress in the cladding begins to turn tensile once mechanical contact occurs at 14 GWd/MTU, and the fuel begins to exert a mechanical force on the cladding. Upon power down at the end of the simulation, some of the stress in the cladding is relieved. For the duplex concept, the hoop-stress evolution is driven by temperature and swelling gradients across the cladding thickness. SiC-SiC composites swell due to irradiation and the amount of swelling is driven by temperature. Thus, a temperature gradient across the SiC cladding results in the inner surface being at much lower compressive stresses as compared to the outer surface. After the fuel-cladding gap closes at 58 GWd/MTU, stresses become tensile as the fuel pushes against the cladding. The contact with the fuel leads to rapid rise in the stresses in both the claddings. The stress levels in the inner composite layer is lower than the proportional limit stress of the SiC composite (~80 MPa [10]), and the stress level in the outer CVD SiC layer is much lower than the tensile strength of the CVD layer (450 MPa [11]). There are opportunities in fuel cladding design and cladding gap size optimization to avoid this hard contact.

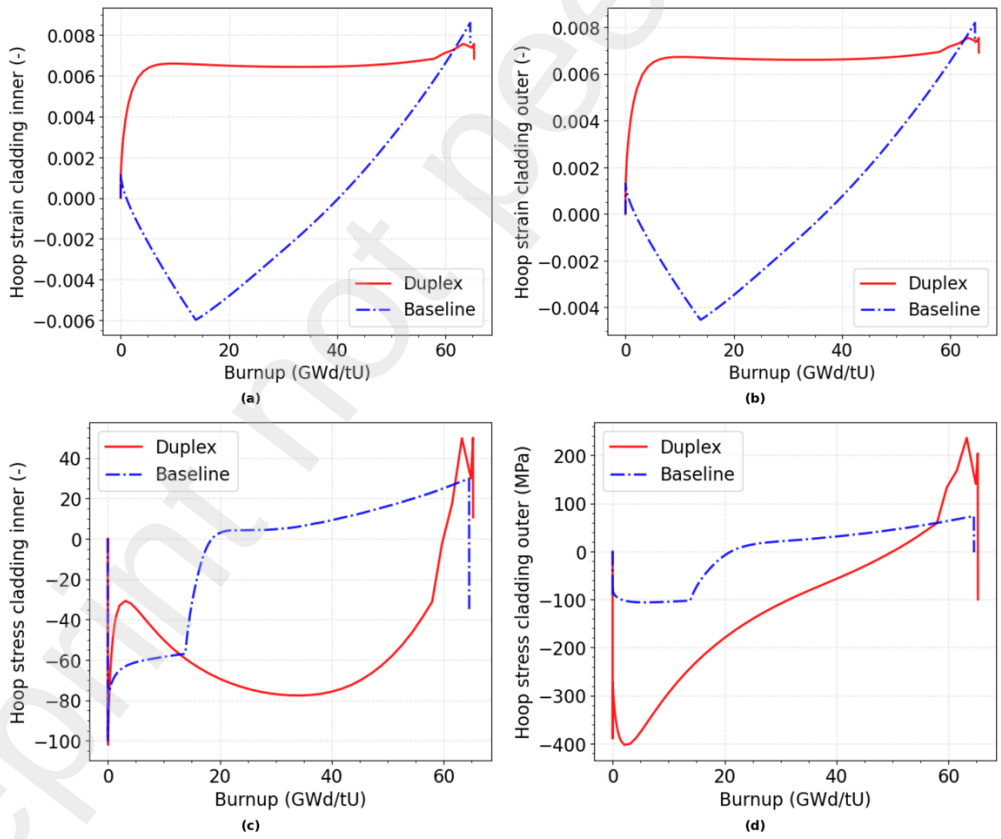

Figure 8. Predictions at the axial midplane of the fuel rod for hoop stress and strain. Hoop strain at the (a) inner and (b) outer cladding surfaces. Hoop stress at the (c) inner and (d) outer cladding surface for the steady-state power case.

4.2 Two-Cycle Case

For the two-cycle case, an average linear heat rate of 35 kW/m was applied to the fuel rod up to 20 GWd/MTU rod average burnup followed by operation at a rod average linear heat rate of 22 kW/m to 62 GWd/MTU rod average burnup. The analysis results for temperature, RIP and FGR for the two-cycle case are provided in Figure 9 and Figure 10. As with the steady-state case, the fuel centerline temperature for the duplex concept behaves as expected due to the improved fuel-cladding gap conductance provided by the liquid metal bonding as shown in Figure 9(a). The RIP versus burnup is presented in Figure 9(b). As noted in the previous section, the initial RIP for the duplex cladding is much smaller than the Zr-4 cladding (0.1 MPa vs 2.0 MPa). The initial RIP increase is higher for the Zr-4 cladding compared to the duplex cladding up to gap closure for the Zr-4 rod after which the rate of increase is higher for the duplex rod. Even though the net FGR for duplex case is smaller (Figure 9(c)), large difference in the RIP ~6.5 MPa (7 MPa in Zr-4 and 0.5 MPa in duplex) decreases to about 2.5 MPa at the EOL because of the small plenum volume available in duplex case. The smaller plenum volume results in a smaller amount of gas needed to generate a certain pressure compared to a larger volume. As expected, the higher initial linear power results in higher peak fuel-centerline temperatures with a resulting increase in FGR and rod pressures reflecting the imposed power history for both cases.

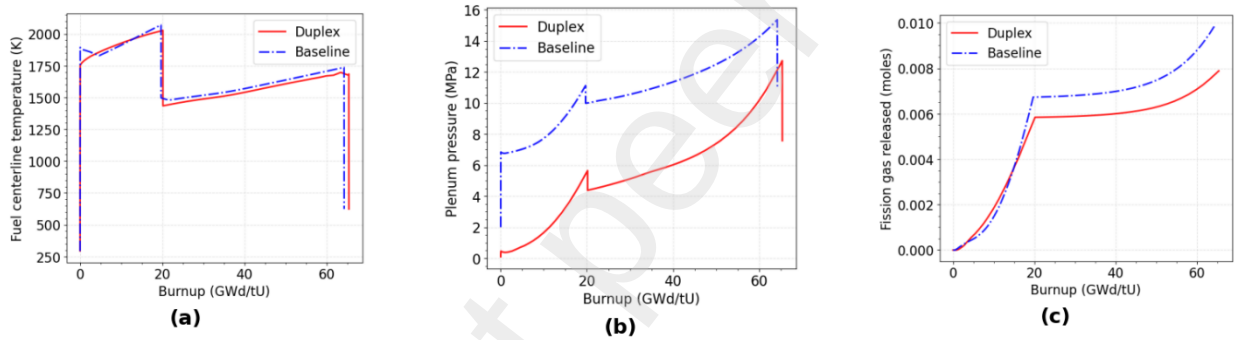

Figure 9. Integral fuel-rod predictions for normal operation: (a) fuel-centerline temperature, (b) rod internal pressure, and (c) fission gas released.

Hoop-strain evolution for both cladding materials are shown in Figure 10(a-b). The Zr-4 case shows cladding creep down until mechanical contact is established with the pellet at approximately 10 GWd/MTU, after which cladding deformation is entirely driven by fuel swelling. The pellet cladding mechanical interaction (PCMI) for the duplex cladding occurs at burnup of 35 GWd/MTU. It should be noted that PCMI for both cladding materials occurs much earlier in the two-cycle case compared to the constant power case because of higher power cycle (35 kW/m vs 22 kW/m). The decrease in the hoop strain at burnup of 20 GWd/MTU is due to the drop in power back to the 22 kW/m level. The effect of power change on hoop strain is significantly less for the duplex case than for the Zr-4 case because for ceramic materials such as SiC the effect of temperature change on its properties is relatively small. Similar observations can be made regarding the hoop stress as shown in Figure 10(c-d) as the effect of the power change is more pronounced on the Zr-4 cladding than the duplex cladding. The stress in the duplex cladding post PCMI rises more rapidly than in the Zr-4 due to relatively high stiffness of the SiC compared to Zr-4. The stress after hard contact is tensile but can be avoided with an optimized design.

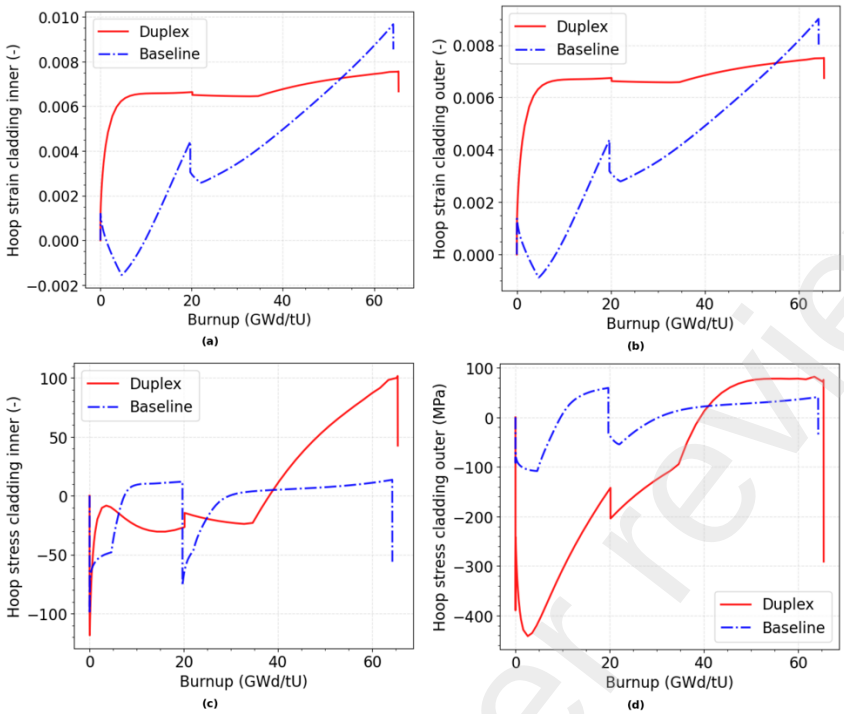

Figure 10. Predictions at the axial midplane of the fuel rod for hoop stress and strain. Hoop strain at the (a) inner and (b) outer cladding surfaces. Hoop stress at the (c) inner and (d) outer cladding surface for the two-cycle power case.

4.3 Early-Life PCI Ramp

One of the concerns with the SiC-SiC composites is performance during AOO ramps. In order to investigate this phenomenon, the AOOs considered in this work consist of an early-life power ramp to induce the pellet-cladding mechanical interaction (PCMI). The analysis results for temperature, plenum pressure and FGR for the early-life power ramp are provided in Figure 11.

The baseline (Zr-4) and duplex cases ramp to approximately the same fuel-centerline temperature with a slight increase through the duration of the case due to the increased gap conductance provided by the liquid metal in the duplex fuel-cladding gap. Plenum pressure and FGR follow similar trends through the duration of the ramp for the duplex and baseline cases. The evolution of the hoop stress and strain at the inner and outer surfaces of the composite layer and baseline cladding for the early-life power ramp are provided in Figure 12. It is evident from the sharp increase in the strain and stresses during the power ramp that pellet-cladding mechanical interaction (PCMI) occurs in both cases. Since the stresses in the composite reach about 80 MPa (Figure 12(c)), there is a possibility of microcracking to occur in the composite layer. The rise in the hoop stress in the outer layer of the cladding, which is made of CVD SiC, is much greater than in the composite layer because the elasticity modulus of the CVD SiC is considerably higher than that of the composite SiC [12],[13].

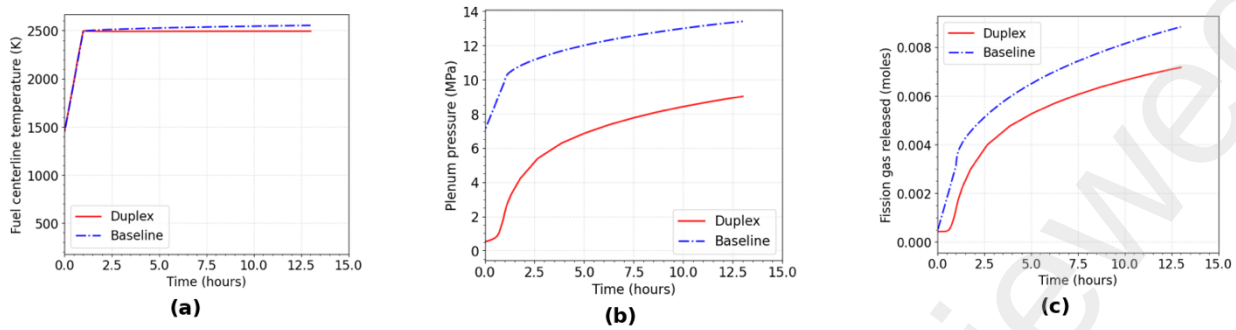

Figure 11. Integral fuel-rod predictions for normal operation: (a) fuel-centerline temperature, (b) rod internal pressure, and (c) fission gas released.

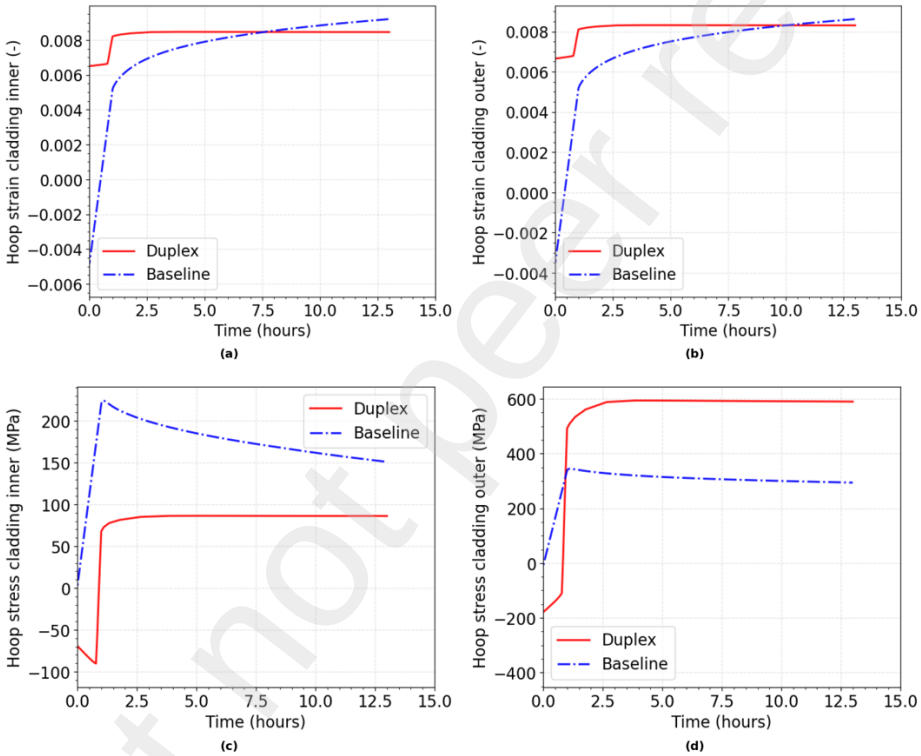

Figure 12. Predictions at the axial midplane of the fuel rod for hoop stress and strain. Hoop strain at the (a) inner and (b) outer cladding surfaces. Hoop stress at the (c) inner and (d) outer cladding surface for the early-life PCI ramp.

4.4 Design-Basis Accidents

The SiC composite claddings are expected to provide excellent passive safety features for DBAs. For the purposes of this evaluation, two DBAs are studied: RIAs and LOCAs.

The analysis results for temperature, RIP, and hoop stresses and strains for the 700 J/g RIA BOL case are provided in Figure 13. The peak power for all concepts occurred at 0.5 sec into the transient. The poor thermal conductivity of UO_2 resulted in the peak fuel temperature being attained slightly after this time and maintained at the maximum temperature for the duration of the simulation. Similarly, the peak RIP was achieved around 0.6 seconds into the transient. Recovery of some thermal expansion over the

remaining approximately 1.4 seconds of the transient resulted in an increase in plenum volume and a subsequent decrease in plenum pressure. The RIP remained below the external coolant pressure.

The hoop stresses and strains are presented in Figure 13 and evolve as expected for this type of transient. For the duplex concept, the interior surface of the composite became extremely hot while the outside surface maintained at a relatively low temperature resulting in a significant thermal strain differential that caused large compressive and tensile stresses at the interior and exterior surface, respectively. Since the stress in the composite layer is compressive, microcracking is not expected to occur. Also, the peak stress in the outer CVD layer is about 230 MPa which is much smaller than the strength of the CVD SiC (~450 MPa [13]), indicating that a RIA with 700 J/g deposition energy does not pose any significant risk to the structural integrity of the duplex cladding. The duplex case did not undergo PCMI during the RIA. The plenum pressure increases greatly for the baseline case compared to the duplex case, which is mainly because of the relatively high initial plenum pressure for the baseline case – the plenum gas expands due to temperature rise leading to increased plenum pressure. The baseline case exhibited PCMI during 0.58 – 0.65 seconds into the transient resulting in an increase in stress and strain.

The second DBA considered in this work was a LOCA simulation. The simulation thermal-hydraulic conditions are based on results from the RELAP thermal-hydraulic analyses discussed in Section 3. The plots of interest include peak fuel-centerline temperature, plenum pressure, and hoop stresses and strains. The results for the BOL LOCA simulation are shown in Figure 14. For the duplex concept, the exterior surface of the composite layer went into slight tension but otherwise handles the transient without failure. The stress in the composite layer reached about 20 MPa, and stress in the CVD layer reached about 75 MPa. These stresses are well below the strengths of the composite (typical proportional limit stress of 80 MPa) and CVD SiC (typical tensile strength of 450 MPa). The baseline concept saw the expected behavior with an increase in pressure until cladding hoop strain starts increasing sharply resulting in a larger plenum volume with decreased pressure to the point of rupture. The hoop strains indicate the likelihood of ballooning as the strains were extremely large. From a safety perspective, the baseline case would result in less-coolable geometry, due to the ballooning, than the duplex concept. Both cases saw a significant reduction in the compressive stress once the blowdown phase was completed. Though not shown in the figure, oxidation resistance was excellent compared to the comparable Zr-4 cladding case.

The results for the EOL LOCA simulation are shown in Figure 15. For this case, the LOCA transient was executed at the end of the standard-power case resulting in a starting condition of a closed fuel-cladding gap, degraded thermal conductivity, and elevated plenum pressures. For the duplex concept, the plenum pressure increased with increasing temperature. The stress in the monolithic and composite layers remained in tension for the duration of the temperature ramp, but the hoop strains remained small. The baseline Zr-4 cladding saw the standard, expected behavior with an increasing hoop strain until the cladding ballooned and failure occurred. The duplex concept survives the transient and maintains its geometry.

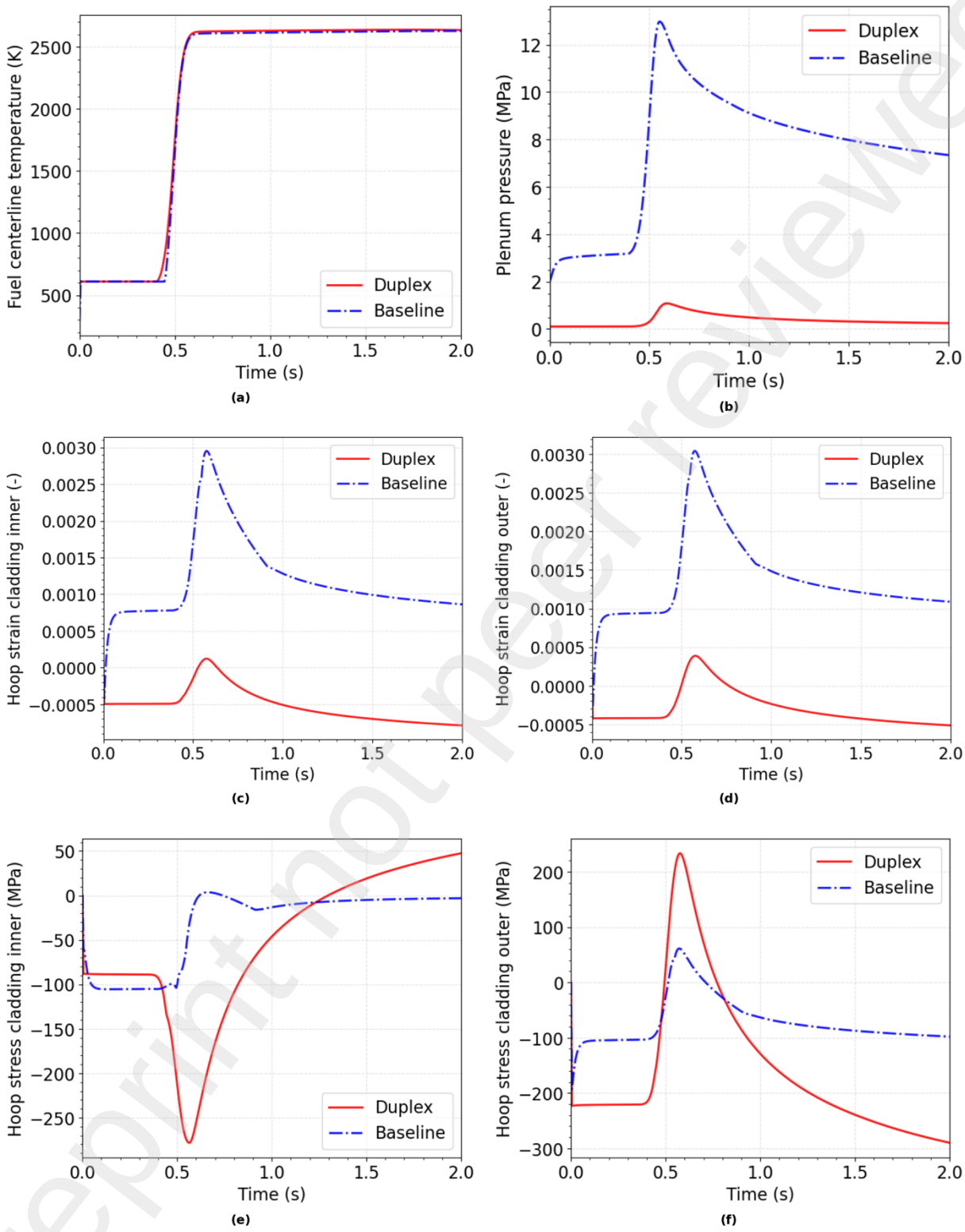

Figure 13. Integral fuel-rod predictions for a 700 J/g pulse: (a) FCT, (b) plenum pressure and hoop strain at the (c) inner and (d) outer cladding surfaces, and hoop stress at the (e) inner and (f) outer cladding surface for the BOL RIA.

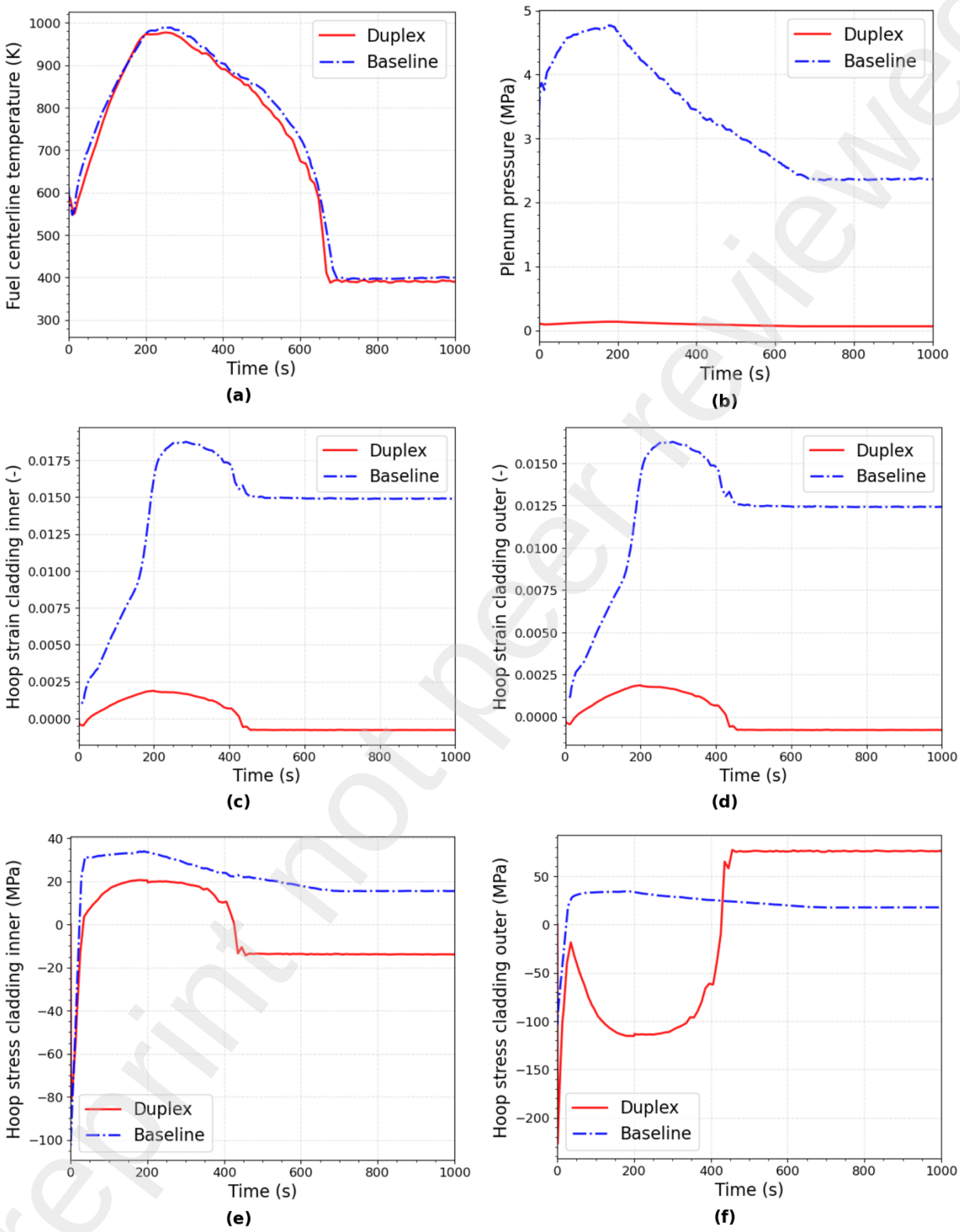

Figure 14. (a) Fuel-centerline temperature, (b) plenum-pressure evolution, (c) inner cladding hoop strain, (d) outer cladding hoop strain, (e) inner cladding hoop stress, and (f) outer cladding hoop stress for the BOL LOCA.

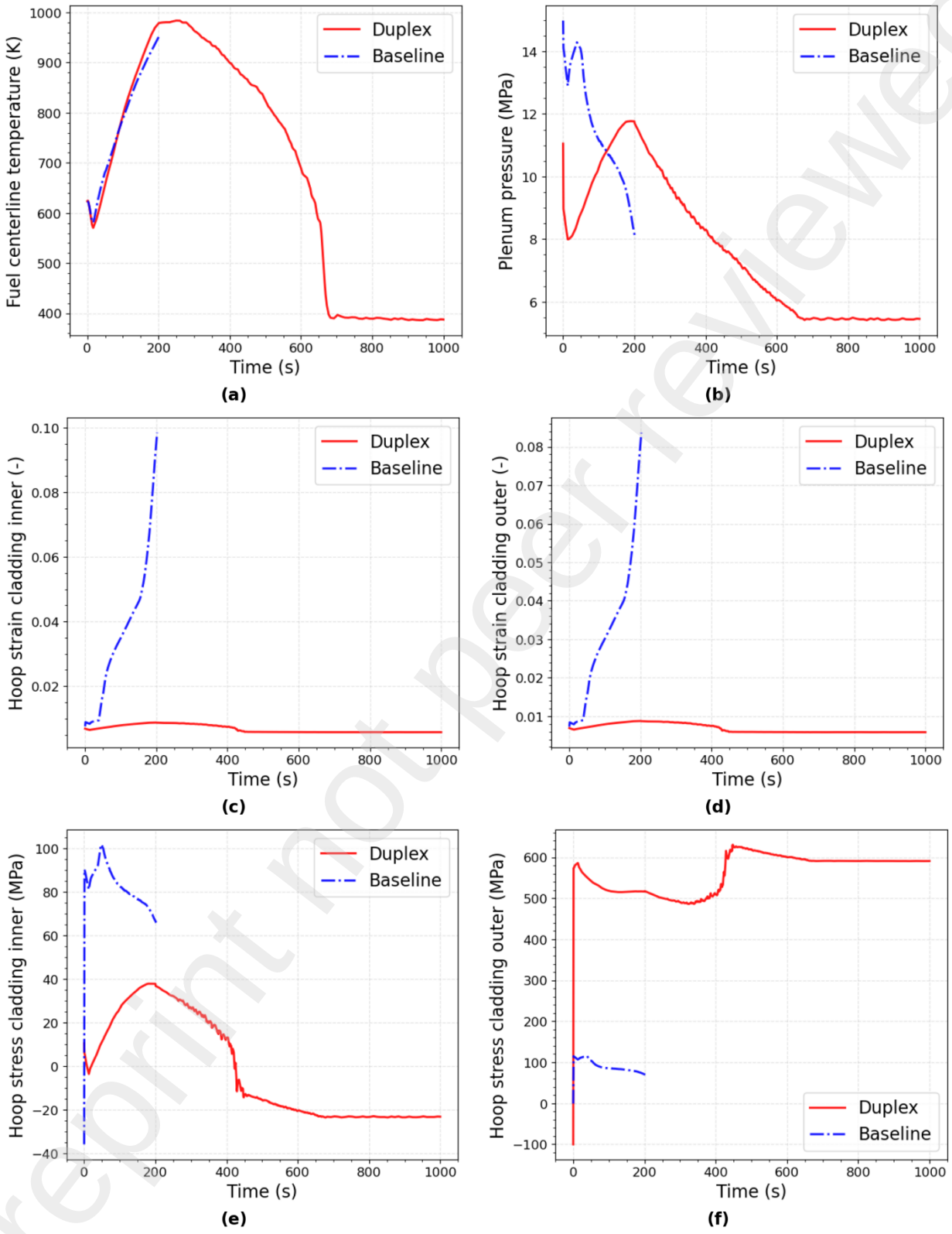

Figure 15. (a) Fuel-centerline temperature, (b) plenum-pressure evolution, (c) inner cladding hoop strain, (d) outer cladding hoop strain, (e) inner cladding hoop stress, and (f) outer cladding hoop stress for the EOL LOCA.

5 CONCLUSION AND FUTURE WORK

This paper reviewed the current material-performance models and fuel performance using the BISON fuel-performance code applied to a current ATF SiC-SiC cladding concept compared to a standard Zr-4 cladding baseline case. For the cases performed in this study, the results indicate superior performance of the duplex cladding compared to the baseline case of Zr-4 cladding. For normal operating conditions, the duplex concept resolved the low thermal conductivity issue of SiC using a liquid-metal bond in the fuel-cladding gap. This approach reduced peak cladding temperatures from the base case until gap closure. An artifact of this approach could result in high plenum pressures as the liquid metal is forced into the plenum as the fuel-cladding gap closes. Future iterations of this design might incorporate a larger initial plenum to improve plenum pressures.

LOCA and RIA simulations were also conducted using BISON. In regard to the RIA evaluation, each fuel-rod concept was subjected to an energy pulse at BOL on fresh fuel. For the duplex concept, the interior surface of the composite becomes extremely hot while the outside surface is maintained at a relatively low temperature. This results in a significant strain differential, causing large compressive and tensile stresses at the interior and exterior surface, respectively. However, the results showed that the 700 J/g energy injection does not pose any significant risk to the structural integrity of the duplex cladding. RIA transients with larger injected energies or occurring at EOL conditions where the fuel-cladding gap would be closed or near closure would be more challenging to the duplex cladding survivability. The results of the LOCA simulation show the duplex concept survives the transient compared to the typical Zr-4 clad fuel behavior with ballooning and bursting. The Zr-4 cladding hoop strains highlight the ballooning effect because the strains are extremely large resulting in a less-coolable geometry compared to the duplex concept. Outstanding oxidation resistance of the monolithic SiC was noted for all the duplex concept evaluation cases.

Some specific concerns are raised by irradiation swelling and low ductility leading to potential PCMI issues for AOOs and RIAs. The SiC material is a ceramic material and maintains its strength at elevated temperatures. However, the stresses in duplex cladding can rise rapidly after fuel comes in contact with the cladding. This is particularly true for the CVD SiC layer which has Young's modulus roughly twice that of composite SiC layer – hence the stress rise rapidly in the CVD layer after fuel pellet cladding contact. This behavior is seen in the ramping evaluation which shows potential fracturing of the SiC-SiC composite of duplex and results from the temperature gradient and subsequent differential swelling across the composite thickness. A design consideration could be to make the composite layer thinner, thereby reducing the temperature graduate across the cladding thickness and reducing composite swelling. It should be noted that the results presented here are valid for the modeled geometry of the duplex cladding which was not optimized for performance. The thickness of the cladding, the relative thickness of the composite SiC layer and the CVD SiC layer can be adjusted to obtain optimized fuel performance. For such optimized geometry, the duplex cladding will perform better than the performance reported here.

In this work the infiltration of the liquid metal gap material into the fuel and cladding and the subsequent effect of their properties was not considered. This effect of liquid metal infiltration should be incorporated in the future work.

CRediT authorship contribution statement

John Alvis: Writing – review & editing, Writing – original draft, Visualization, Methodology, Investigation, Data curation, Conceptualization. Gyanender Singh: Writing – review & editing, Writing – original draft, Methodology, Formal analysis, Software. Kyle Gamble: Writing – review & editing, Writing – original draft, Methodology, Formal analysis, Software. David Kamerman: Writing – review & editing Supervision, Resources, Project administration, Funding acquisition. Seokbin Seo: Writing – review & editing, Writing – original draft, Software. Katheren Nantes: Software

Declaration of competing interest

The authors declare that they have no known competing financial interests or personal relationships that could have appeared to influence the work reported in this paper.

Acknowledgements

This manuscript has been authored by Battelle Energy Alliance, LLC, under Contract No. DE-AC07-05ID14517 with the U.S. Department of Energy, with funding from the Advanced Fuels Campaign program. The U.S. Government retains and the publisher, by accepting the article for publication, acknowledges that the U.S. Government retains a nonexclusive, paid-up, irrevocable, worldwide license to publish or reproduce the published form of this manuscript, or allow others to do so, for U.S. Government purposes. This research made use of the resources of the High Performance Computing Center at Idaho National Laboratory, which is supported by the Office of Nuclear Energy of the U.S. Department of Energy and the Nuclear Science User Facilities under Contract No. DE-AC07-05ID14517.

The raw/processed data required to reproduce these findings cannot be shared at this time due to technical or time limitations.

Data availability

Data will be made available on request.

6 REFERENCES

[1] Yueh, K., and Terrani,K.A. 2014. “Silicon carbide composite for light water reactor fuel assembly applications .” *J. Nucl. Mater.* 448(1-3):380-388.

[2] Bragg-Sitton, S.M. 2012. “Light Water Reactor Sustainability Program Advanced LWR Nuclear Fuel Cladding System Development Technical Program Plan.” Technical Report INL/MIS-12-25696. Idaho National Laboratory.

[3] Naslain, R. 2004. “Design, preparation and properties of non-oxide CMCs for application in engines and nuclear reactors: an overview.” Sci. Technol., 64(1):155-17

[4] Cinbiz, M., T. Koyanagi, G. Singh, Y. Katoh, K. Terrani, and N. Brown. “Failure behavior of SiC/SiC composite tubes under strain rates similar to the pellet-cladding mechanical interaction phase of reactivity-initiated accidents.” J. Nucl. Mater. 514(1):66-73. https://doi.org/10.1016/j.jnucmat.2018.11.023.

[5] Williamson, R. L., J. D. Hales, S. R. Novascone, G. Pastore, K. A. Gamble, B. W. Spencer, et.al. 2021. “BISON: A Flexible code for advanced simulation of the performance of multiple nuclear fuel forms.” *Nucl. Technol.* 207(7):954–980. https://doi.org/10.1080/00295450.2020.1836940.

[6] O’Donnell, G. M., H. H. Scott, and R. O. Meyer. 2001. A Comparative Analysis of LWR Fuel Designs. NUREG-1754, U.S. Nuclear Regulatory Commission, Office of Nuclear Regulatory Research, Washington, D.C.

[7] Katoh, Y., K. Ozawa, C. Shih, T. Nozawa, R. J. Shinavski, A. Hasegawa, and L. L. Snead. 2014. “Continuous SiC fiber, CVI SiC matrix composites for nuclear applications: Properties and irradiation effects.” *J. Nucl. Mater.* 448(1):448–476. https://doi.org/10.1016/j.jnucmat.2013.06.040.

[8] Snead, L. L., T. Nozawa, Y. Katah, T.-S. Byun, S. Kondo, and D. A. Petti. 2007. “Handbook of SiC properties for fuel performance modeling.” *J. Nucl. Mater.* 371(1):329–377. https://doi.org/10.1016/j.jnucmat.2007.05.016.

[9] Nozawa, T., K. Ozawa, Y.-B. Choi, A. Kohyama, and H. Tanigawa. 2012. “Determination and prediction of axial/off-axial mechanical properties of SiC/SiC composites.” *Fusion Eng. Des.* 87(5–6):803–807. https://doi.org/10.1016/j.fusengdes.2012.02.026.

[10] Snead, M., Y. Katoh, T. Koyanagi, and G. P. Singh. 2017. SiC/SiC Cladding Materials Properties Handbook. ORNL/TM-2017/385, Oak Ridge National Laboratory, Oak Ridge, TN. https://doi.org/10.2172/1399957.

[11] Snead, L. L., S. J. Zinkle, and D. P. White. 2005. "Thermal conductivity degradation of ceramic materials due to low temperature, low dose neutron irradiation." *J. Nucl. Mater.* 340(2–3):187–202. https://doi.org/10.1016/j.jnucmat.2004.11.009.

[12] Stone, J. G., P. Schleicher, C. P. Deck, G. M. Jacobsen, H. E. Khalifa, and C. A. Back. 2015. "Stress analysis and probabilistic assessment of multi-layer SiC-based accident tolerant nuclear fuel cladding." *J. Nucl. Mater.* 466:682–697. https://doi.org/10.1016/j.jnucmat.2015.08.001.

[13] Allison, C. M., G. A. Berna, R. Chambers, E. W. Coryell, K. L. Davis, D. L. Hagrman, et al. 1995. SCDAP/RELAP5/MOD 3.1 Code Manual: MATPRO – A Library of Materials Properties for Light-Water-Reactor Accident Analysis. Volume 4. NUREG/CR–6150, EGG–2720, Idaho National Engineering Laboratory, Idaho Falls, ID.

[14] Siefken, L. J., E. W. Coryell, E. A. Harvego, and J. K. Hohorst. 2001. SCDAP/RELAP5/MOD3.3 Code Manual: MATPRO – A Library of Materials Properties for Light-Water-Reactor Accident Analysis. NUREG/CR–6150, Volume 4, Revision 2, U.S. Nuclear Regulatory Commission, Washington, D.C.

[15] Katoh, Y., T. Koyanagi, J. L. McDuffee, L. L. Snead, and K. Yueh. 2018. "Dimensional stability and anisotropy of SiC and SiC-based composites in transition swelling regime." *J. Nucl. Mater.* 499:471–479. https://doi.org/10.1016/j.jnucmat.2017.12.009.

[16] Erbacher, F. J., H. J. Neitzel, H. Rosinger, H. Schmidt, and K. Wiehr. 1982. "Burst criterion of Zircaloy fuel claddings in a loss-of-coolant accident." In Franklin, D. G. (ed.) *Zirconium in the Nuclear Industry, Fifth Conference*, ASTM STP 754, 271–283. American Society for Testing and Materials, West Conshohocken, PA.

[17] Terrani, K. A., B. A. Pint, C. M. Parish, C. M. Silva, L. L. Snead, and Y. Katoh. 2014. "Silicon carbide oxidation in steam up to 2 MPa." *J. Am. Ceram. Soc.* 97(8):2331–2352. https://doi.org/10.1111/jace.13094.

[18] INL. n.d. BISON Documentation webpage. Available at: https://mooseframework.inl.gov/bison/source/materials/tensor_mechanics/ZryCreepLOCAUpdate.html (accessed February 29, 2024).

[19] Markiewicz, M. E., and F. J. Erbacher. 1988. Experiments on Ballooning in Pressurized and Transiently Heated Zircaloy-4 Tubes. KfK–4343, Kernforschungszentrum Karlsruhe GmbH, Germany. Available at: https://publikationen.bibliothek.kit.edu/270025905/3813281 (accessed May 10, 2024).

[20] Geelhood, K. J., C. E. Beyer, and W. G. Luscher. 2008. PNNL Stress/Strain Correlation for Zircaloy. PNNL-17700, Pacific Northwest National Laboratory, Richland, WA.

[21] The RELAP5-3D Code Development Team. 2012. RELAP5-3D Code Manual Volume I: Code Structure, System Models and Solution Methods. INL-EXT-98-00834-V1, Revision 4.2, Idaho National Laboratory, Idaho Falls, ID.

[22] Garzarolli, F. and Garzarolli, M., 2012. PWR Zr alloy cladding water side corrosion. *Advanced Nuclear Technology International, Mölnlycke, Sweden*.

[23] Schanz, G., 2003. *Recommendations and supporting information on the choice of zirconium oxidation models in severe accident codes* (Vol. 6827). FZKA.

[24] Giudicelli, G., Lindsay, A., Harbour, L., Icenhour, C., Li, M., Hansel, J.E., German, P., Behne, P., Marin, O., Stogner, R.H. and Miller, J.M., 2024. 3.0-MOOSE: Enabling massively parallel multiphysics simulations. *SoftwareX*, *26*, p.101690.

[25] D. Kamerman, N. Woolstenhulme, D. Imholte, A. Fleming, C. Jensen, C. Folsom, C. Woolum, K. Tritthart, J. Schulthess, D. Wachs. 2021. "Performance of uranium silicide fuel and silicon-carbide composite cladding in reactivity-initiated accident testing." Ann. Nucl. Energy, 160, Article 108410. https://doi.org/10.1016/j.anucene.2021.108410.

[26] Schulthess, J., Kamerman, D., Winston, A., Pomo, A., Trowbridge, T., Pu, X., Woolstenhulme, N., Imholte, D., Jensen, C., & Wachs, D. (2022). "Post-transient examination of performance of uranium silicide fuel and silicon-carbide composite cladding under reactivity-initiated accident conditions." *J. Nucl. Mater.*, *560*, Article 153520. https://doi.org/10.1016/j.jnucmat.2022.153520.

[27] Hill, R., 1948. A theory of the yielding and plastic flow of anisotropic metals. *Proceedings of the Royal Society of London. Series A. Mathematical and Physical Sciences*, *193*(1033), pp.281-297.

[28] Singh, G., Recuero, A., Gamble, K., Hales, J., Jacobsen, G. and Ellis, C., Pseudo Ductility Model for SiC-SiC Cladding (under preparation).

[29] Katoh, Y., L.L. Snead, T. Nozawa, S. Kondo, J.T. Busby. 2010. "Thermophysical and mechanical properties of near-stoichiometric fiber CVI SiC/SiC composites after neutron irradiation at elevated temperatures." *J. Nucl. Mater.* 403(1-3): 48-61. https://doi.org/10.1016/j.jnucmat.2010.06.002.